AIP | APL Materials

NOW INDEXED IN THOMSON REUTERS DATABASES

Research Update: Physical and electrical characteristics of lead halide perovskites for solar cell applications

Simon A. Bretschneider, Jonas Weickert, James A. Dorman, and Lukas Schmidt-Mende

Citation: APL Materials **2**, 040701 (2014); doi: 10.1063/1.4871795
View online: http://dx.doi.org/10.1063/1.4871795
View Table of Contents: http://scitation.aip.org/content/aip/journal/aplmater/2/4?ver=pdfcov
Published by the AIP Publishing

APL MATERIALS **2**, 040701 (2014)

Research Update: Physical and electrical characteristics of lead halide perovskites for solar cell applications

Simon A. Bretschneider, Jonas Weickert, James A. Dorman, and Lukas Schmidt-Mende[a]
Department of Physics, University of Konstanz, P.O. Box 680, 78467 Constance, Germany

(Received 24 February 2014; accepted 3 April 2014; published online 23 April 2014)

The field of thin-film photovoltaics has been recently enriched by the introduction of lead halide perovskites as absorber materials, which allow low-cost synthesis of solar cells with efficiencies exceeding 16%. The exact impact of the perovskite crystal structure and composition on the optoelectronic properties of the material are not fully understood. Our progress report highlights the knowledge gained about lead halide perovskites with a focus on physical and optoelectronic properties. We discuss the crystal and band structure of perovskite materials currently implemented in solar cells and the impact of the crystal properties on ferroelectricity, ambipolarity, and the properties of excitons. [http://dx.doi.org/10.1063/1.4871795]

The recent development of lead halide perovskite solar cells is remarkable. The first results were published in 2009 with efficiencies close to 4% using an electrolyte as hole transport material.[1] In 2012, two publications[2,3] increased the efficiency, peaking around 10%, using device geometries similar to a solid-state dye-sensitized solar cell. While both publications used a mesoporous nanoparticle network, the concepts were fundamentally different. The Grätzel group used sintered TiO_2 nanoparticles as an electrode material, while the Snaith group replaced this material with a nanostructured Al_2O_3 film, which only serves as a scaffold layer and does not allow charge transport due to the insulating character of Al_2O_3. In addition to the different nanostructure, two different lead halide perovskites were used, $CH_3NH_3PbI_3$[2] and $CH_3NH_3PbI_{3-x}Cl_x$.[3] Latest results explain why these two different concepts peak at similar conversion efficiencies up to 16.2%[4–8]: in both cases the charge carrier diffusion length exceeds the absorption depth, simultaneously allowing for highly efficient photon harvesting and small losses during charge collection. However, the charge generation and transport properties in lead halide perovskites are not fully understood. Within the last year, several different concepts for the utilization of the unique properties of the lead halide perovskite were used, such as thin-film planar heterojunctions,[9–12] distributed heterojunctions with mesoporous TiO_2, ZrO_2, and Al_2O_3 nanostructures,[2,5,13–21] ordered TiO_2 and ZnO distributed heterojunctions,[22] and depleted heterojunctions.[23] The planar heterojunction design is mostly used for $CH_3NH_3PbI_{3-x}Cl_x$, although in a recent publication $CH_3NH_3PbI_3$ has been used in a planar heterojunction design,[5,24] which otherwise is still mainly applied on nanostructured TiO_2 electrodes. The performance of perovskite solar cells strongly depends on the crystallinity of the perovskite layer. Recent results show that only a minority of the perovskite in a mesoporous nanostructure has medium range crystalline order, while the majority consists of nanoparticle-like perovskite crystallites,[25] in contrast to planar heterojunction cells, where the crystallites are much larger, several hundred nanometers up to micrometer scale.[5,11,24] For fabrication of different cells, vapor deposition techniques[11,24] as well as one[2,3,13,18] and two-step[14,26] solution-processed techniques have been used. The fabrication was recently reviewed by Snaith,[27] Park,[28] and Kim *et al.*[29] This research update discusses the interplay

[a]Author to whom correspondence should be addressed. Electronic mail: lukas.schmidt-mende@uni-konstanz.de

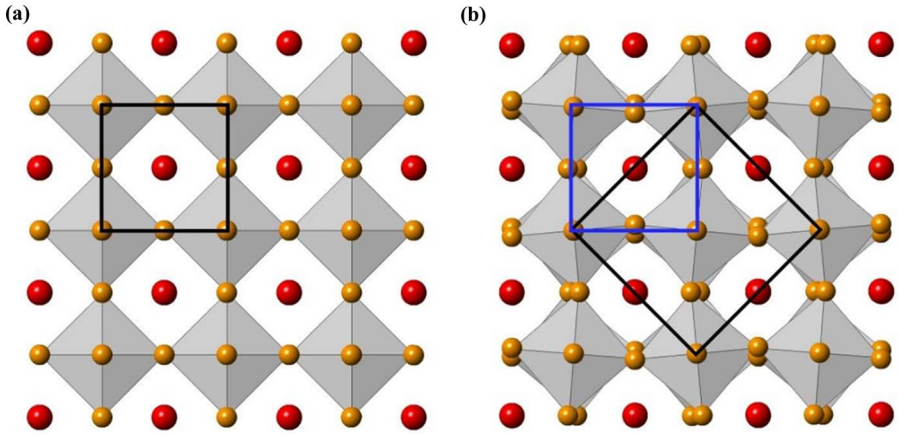

FIG. 1. Pseudocubical (a) and tetragonal (b) lattice of lead halide perovskites; the black cell shows the unit cell. The red points are the A cations, yellow halide atoms (X), the grey octahedra centered to metal cation (M). The blue cells show the pseudocubical lattice in the tetragonal phase. Reproduced by permission from Eperon *et al.* Energy Environ. Sci. 7, 982 (2014). Copyright 2014 The Royal Society of Chemistry.

of the physical and electronic structure of lead halide perovskites with respect to their photovoltaic applications.

To date, lead halide perovskites have been implemented in photovoltaics mainly as absorbers and, in some cases, as charge transport materials. The perovskite structure is commonly understood as that of the mineral $CaTiO_3$[30] or, more generally, a compound material of stoichiometry AMX_3. Inorganic perovskites have three-dimensional structures based on corner sharing anionic MX_6 octahedra, the *X*-atoms sit in the corners, and the *M*-atom in middle of the octahedra. The *A*-cations are located at interstices, surrounded by 8 octahedra in the cuboctahedral gap.[31] The perovskite only forms because there is a large difference in sizes between the A and M cations. A majority of the known perovskite materials are fully inorganic, e.g., $BaSnO_3$, $BiFeO_3$, or $SrTiO_3$ and feature a wide range of properties such as piezo-, ferro-, and pyroelectricity, giant magnetoresistance, an abnormal photovoltaic effect and superconductivity.[32,33] For photovoltaic applications, two types of perovskites are being used: inorganic $CsSnI_3$ as a hole conducting material[34] and lead halide perovskites with organic cations. In case of the lead halide perovskites, the lead and halide atoms form the inorganic octahedron acting as the anion, while the organic cation, e.g., methylammonium ($CH_3NH_3^+$) resides in the interstices. The structure of the inorganic/organic perovskite is decisively determined by the size of the organic cation. Small cations like methylammonium maintain a three-dimensional structure of the perovskite, larger cations, e.g., organic molecules containing phenyl-groups, will result in a layered structure with inorganic sheets alternating with organic layers.[35] These sheets are connected by Van der Waals forces. The lead halide perovskite $CH_3NH_3PbI_3$ has four solid phases, three of them perovskite-like. The perovskite-phases are named with α, β, and γ and the non-perovskite δ-phase.[31] α is the high-temperature phase for temperatures $T > 327$ K[36] and has a pseudocubical crystal structure. A scheme of the unit cell is shown in Fig. 1(a). The inorganic perovskite $CsSnI_3$ has cubic structure (space group $Pm\bar{3}m$) for the high-temperature phase.[31] Cubic structures allow only one formula unit per unit cell,[36] therefore perovskites with cations such as $CH_3NH_3^+$ cannot obtain the cubic structure.[33] For temperatures lower than 327 K, the perovskite undergoes a phase transition to the tetragonal β-phase (noncentrosymmetric, space group I4 cm[25,33] with lattice parameters $a = 8.855$ Å and $c = 12.659$ Å[1]). The exact parameters depend on molecular orientation.[37] In the α- and β-phase, the methylammonium cations are disordered. Ferroelectric response like capacitance and non-ohmic behavior, which might be responsible for hysteretic behavior in the current/voltage curves, could be attributed to the reorientation of the methylammonium cations in an external field and the resistance of the inorganic lead-iodide lattice.[19,33] Due to the tilting of the octahedra during the phase transition from α- to β-phase (tilting angle 16.4° at 293 K), the unit cell doubles its length, thus octupling its volume and forming a super-cell.[33] In Fig. 1(b), a larger unit cell of the tetragonal phase of $CH_3NH_3PbI_3$ is shown due to the tilting of the octahedra.

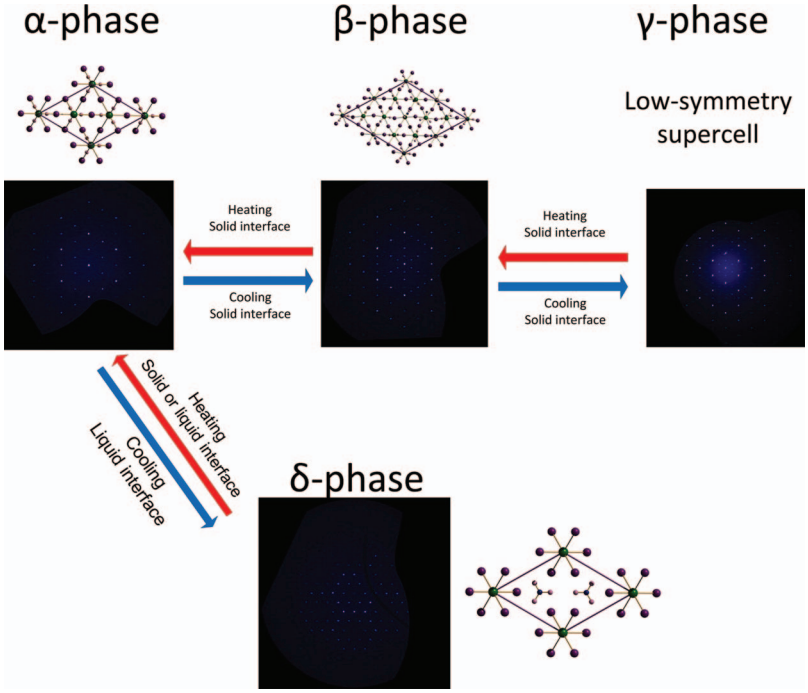

FIG. 2. Scheme ([006] view) of phase transitions of lead halide perovskite. The high-temperature α-phase has two possible phase transitions, for dry crystals to the β- (T < 327 K) and γ-phase (T < 162 K) or in the presence of, e.g., a solvent to the δ-phase for temperature below ~360 K. Reprinted with permission from Stoumpos *et al.*, Inorg. Chem. **52**(15), 9019 (2013). Copyright 2014 American Chemical Society.

The bromine equivalent of $CH_3NH_3PbI_3$, $CH_3NH_3PbBr_3$, has a cubic structure (space group $Pm3m$) at room temperature. The different structure arises from different ion sizes of bromine and iodine in a six-fold coordination.[20] For temperatures below 162 K, the perovskite undergoes a phase transition to a orthorhombic γ-phase (space group $Pmc2_1$[36]), where the methylammonium cations are ordered. During the phase transitions from α to β and γ, the octahedra are tilted and deform from the ideal octahedron with respect to cubic phase. For decreasing temperatures, tilting and deformation effects increase.[31] Phase transitions between the α-, β-, and γ-phases occur in the solid phase, while the transition to the non-perovskite δ-phase happens in the presence of solvents.[33] A schematic phase diagram of the different perovskite phases is shown in Fig. 2.

The perovskite structure is based on ionic bonds in a way that the total charge is balanced, thus forming anionic corner-connected inorganic octahedra via covalent bonds with organic cations in the cuboctahedral gap.[39,40] Another structural effect arises from the stereochemical *lone pair* $6s^2$ electrons. These lone pair electrons influence the structure of the perovskite through the relocation of the lead atom, which leads to a variation of bonding length within the octahedra.[36,37] Beyond the pure lead halide perovskites, another type of perovskite was used for photovoltaic applications, namely, the mixed halide perovskite, where the iodine is replaced partly with either chlorine $CH_3NH_3PbI_{3-x}Cl_x$,[3,12,13] which is derived from the pure halide perovskite $CH_3NH_3PbI_3$ via apical substitution of the iodine atom with a chlorine atom. The incorporation of the chlorine atom adds a small perturbation to the equatorial iodine atoms including a small contraction of the octahedron.[11,40] The energy required for insertion of a chlorine atom is 160 meV.[16,19]

The amount of chlorine included in the lead-iodine perovskite is not clear yet. The majority of literature found small amounts of chlorine in the perovskite, in the range 2%–4%[12,15] despite a CH_3NH_3I and $PbCl_2$ (with dimethylformamide (DMF) as a solvent) precursor ratio of 3:1.[3,13,15] For a precursor ratio of 1:1, a separate $CH_3NH_3PbCl_3$ phase can be observed. A separate phase for high chlorine concentrations and DMF as a solvent indicates a low solubility of chlorine in the iodine derivative, supported by the segregated $CH_3NH_3PbCl_3$.[15] The use of dimethyl sulfoxide

(DMSO) as a solvent enhances the amount of chlorine in the $CH_3NH_3PbI_{3-x}Cl_x$. Using DMSO, a chlorine/iodine ratio of 2:1 was measured.[9] Another mixed halide perovskite is $CH_3NH_3PbI_{3-x}Br_x$.[20] The energy required to insert a bromine atom into the lead-iodine lattice is smaller (50 meV[40]) compared to the chlorine due to larger ion radii differences between iodine (220 pm[13]) and chlorine (181 pm[41]) compared to bromine (196 pm[20]). The small energy enables the tuning of the bromine content between a pure iodine perovskite (x = 0) and a pure bromine perovskite (x = 3).[20] When increasing the fraction of bromine, the $CH_3NH_3PbI_{3-x}Br_x$ perovskite undergoes a phase transition from tetragonal to cubic. X-ray diffraction indicates a turnover fraction of about 20% bromine.[20]

In addition to the structural similarities of pure and mixed lead halide perovskites, the electronic properties are very similar[13,18] since the band structure close to the bandgap is dominated by lead and iodine orbitals.[40,42] This is a result of the electronic structure of the organic-inorganic perovskite with a network formed of alternating organic cations and the inorganic octahedra. The bandgap of the perovskite is dominated by the smaller energy gap of the inorganic lead halide lattice, while the larger energy difference between the lowest unoccupied molecular orbital and the highest occupied molecular orbital of the organic cations have a weaker contribution.[43] The conduction band minimum is dominated by non-bonding 6*p*-orbitals of the lead, the valence band maximum by anti-bonding hybridized lead 6*s*- iodine 5*p* orbitals.[37,42,44] Bromine and chlorine states are located at energies below the valence band edge and do not contribute much in case of the mixed halide perovskites, as determined via first principle investigations, especially the type of halide (Cl^-, Br^-, I^-) sitting in the apical positions of the octahedra has little contribution to the number of states near the band edges.[40] The molecular units of methylammonium form σ-bonds deep in the valence band and do not hybridize with the inorganic octahedra for small bias, thus providing mostly electrostatic charge compensation.[44] For the lead contribution, the huge spin–orbit coupling of the heavy lead atoms is even more important. Simulations show a large difference for the bandgap, with and without attention to the spin–orbit coupling of the lead. The energy difference between $3P^2$ and $3P^0$ level of the lead with and without recognition of the spin–orbit coupling exceeds more than 1 eV.[42] The large contribution of the spin–orbit coupling to the conduction band maximum is another explanation why replacement of the apical atoms of the octahedron changes little in the band structure.[45] In addition to the spin–orbit effects, relativistic effects are also important for lead: valence and conduction band near the band extrema deviate from the parabolic form, resulting in a dependence of effective masses of temperature and possible doping.[44] One possible doping mechanism has been suggested since photoelectron spectroscopy measurements show traces of metallic lead in both $CH_3NH_3PbI_3$ and $CH_3NH_3PbI_{3-x}Cl_x$.[9,46] The reduction of lead might arise from loss of iodine atoms, e.g., through formation of I_2.[46] The presence of traces of metallic lead could possibly introduce weakly bound electrons to the crystal, i.e., result in n-doping of the material. The band composition, due to the structure of the organic-inorganic perovskite, offers the possibility of bandgap engineering and tailoring of carrier mobility using either different organic cations or by variation of the inorganic lattice.[47] $CH_3NH_3PbI_3$ is a direct semiconductor with a bandgap of 1.5 eV with the conduction band minimum at −3.93 eV and the valence band maximum at −5.43 eV[2], with respect to the vacuum level. In Fig. 3, a calculated band structure for $CH_3NH_3PbI_3$ using different algorithms is shown. The bandgap for the quasiparticle self-consistent GW approximation (QSGW; solid lines) is slightly overestimated compared to experimental data (1.5–1.6 eV[2,15]), while the local density approximation (LDA, dashed line) underestimates the bandgap energies.[44]

When chlorine is incorporated in $CH_3NH_3PbI_3$, the bandgap remains direct and increases slightly to 1.55 eV with a conduction band minimum of −3.75 eV and a valence band maximum of −5.3 eV.[48] The energy difference between the Fermi energy and the valence band maximum of $CH_3NH_3PbI_{3-x}Cl_x$ (2.2% chlorine ratio) was measured to be 1.1 eV, indicating a weak n-type or intrinsic semiconductor[12] in contrast to $CH_3NH_3PbI_3$, which was reported to be a p-type semiconductor.[23] The direct bandgaps of $CH_3NH_3PbBr_3$ and $CH_3NH_3PbCl_3$ are 2.32 eV[20] and 3.1 eV, respectively.[49] For a direct comparison between $CH_3NH_3PbI_3$ without chlorine and with chlorine with different precursor concentrations (without any chloride, precursor ratios $CH_3NH_3I/PbCl_2$ 3:1 and 1:1[15]), the bandgap for all perovskites is 1.6 eV, despite the larger bandgaps expected from the larger chlorine contribution. The change of the bandgap due to the chlorine is within the tolerance of the optical measurement.[15] The reason for the reduced bandgap for higher chlorine concentrations

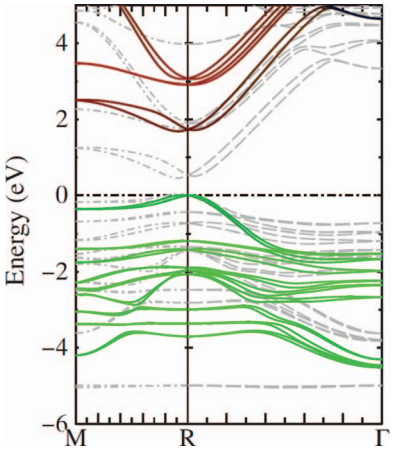

FIG. 3. Calculated band structure for $CH_3NH_3PbI_3$ for QSGW (solid lines) and LDA (dashed lines) approximations. Zero energy marks the valence band maximum. The color of the bands is related to the related orbitals: green I 5p, red Pb 6p, and blue Pb 6s, bands closer to the bandgaps are darker due to hybrid orbitals. R and M are zone-boundary points close to $\left(\frac{1}{2}, \frac{1}{2}, 0\right)$ and $\left(\frac{1}{2}, \frac{1}{2}, \frac{1}{2}\right)$, respectively. Reprinted with permission from Brivio *et al.*, Phys. Rev. B **89**, 155204 (2014). Copyright 2014 American Physical Society.

(stoichiometric ration of 3:1) could be a different structure of the perovskite. For low chlorine concentrations, density functional theory calculations indicate a more disordered structure compared to higher concentrations.[15] In contrast to the relatively small changes in bandgaps in iodine/chlorine perovskite the combination of iodine and bromine as halides in $CH_3NH_3PbI_{3-x}Br_x$ allows for the tuning of the bandgap between 1.5 and 2.32 eV[20] due to the small replacement energy of iodine atoms with bromine. A recently published combination of a chlorine/bromine perovskite $CH_3NH_3PbBr_{3-x}Cl_x$ can increase the bandgap even further.[21] In addition to the variation of the bandgap by using different configurations of the inorganic octahedra of the perovskite, the organic cation offers another setscrew for the energy gap. Replacement of the methylammonium cation with a formamidinium cation $HC(NH_2)_2^+$ reduced the bandgap to 1.47 eV due to a change of the bond lengths of the inorganic octahedra.[38,50] The bromide equivalent has a bandgap of 2.23 eV.[38] Very high open-circuit voltages, up to 1.1 eV[11] have been measured for halide perovskite solar cells. A loss-in-potential of 0.45 eV[27] is slightly smaller than for the best inorganic materials like GaAs or crystalline silicon. The origin of this low loss-in-potential is not fully understood yet and currently under investigation by different groups. The intrinsic carrier density in the lead halide perovskite was measured to be 10^9 cm^{-3}, similar to intrinsic semiconductors like silicon,[33] however the electron mobility is much lower with 66 cm^2/Vs.[33] Recent measurements for the charge mobility in $CH_3NH_3PbI_{3-x}Cl_x$ set a lower bound of 11.6 cm^2/Vs.[51] Upon replacement of the lead with tin to form $CH_3NH_3SnI_3$ (bandgap 1.21–1.35 eV depending on preparation), the calculated carrier mobility increases drastically (electron mobility 2320 cm^2/Vs; hole mobility 322 cm^2/Vs[33]). This more metal-like behaviour can be attributed to oxidation of tin atoms in contrast to the lead atoms, which are unable to be oxidized in the iodine environment.[33]

The energy bands of the lead halide perovskites represent the ambipolar characteristic, since valence band and conduction band are almost mirrored.[40] Theoretical estimation of the effective masses for electrons and holes in $CH_3NH_3PbI_3$ in the pseudo-cubic α-phase at the valence band maximum and conduction band minimum including the effects of spin–orbit coupling results in $m_e^* = 0.23\ m_0$ and $m_h^* = 0.29\ m_0$.[52] These predicted effective masses do not include elastic scattering effects; they therefore correspond to a maximum effective mass with minimal scattering effects.[52] The diffusion length (L_D) is calculated from the equation $L_D = \sqrt{D\tau_e}$, where D is the diffusion constant and τ_e the recombination lifetime without a photoluminescence quenching material, which is fitted from the photoluminescence decay shown in Figs. 4(c) and 4(d). The diffusion length measured via photoluminescence decay experiments for electrons and holes in the mixed halide perovskite $CH_3NH_3PbI_{3-x}Cl_x$ are ~1 μm and ~1.2 μm, respectively.[7] The diffusion length of both charge carriers for $CH_3NH_3PbI_3$

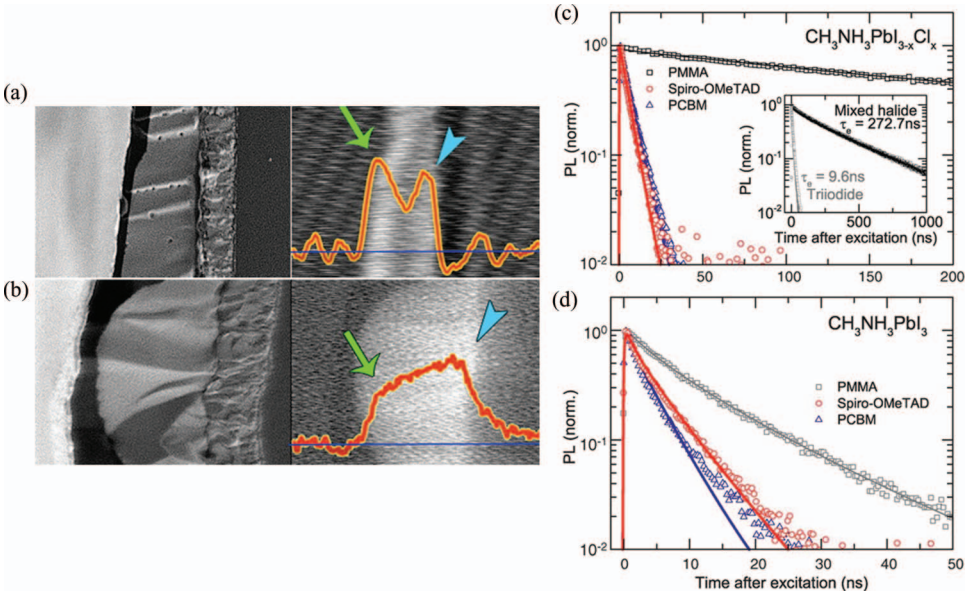

FIG. 4. Electron beam induced current measurement of $CH_3NH_3PbI_{3-x}Cl_x$ (a) and $CH_3NH_3PbI_3$ (b) and photoluminescence decay measurements of the peak emission wavelength for $CH_3NH_3PbI_{3-x}Cl_x$ (c) and $CH_3NH_3PbI_3$ (d). The blue and green arrows indicate the peak of charge separation at the perovskite/electron conductor and perovskite/hole transporter, respectively. Reprinted with permission from Edri *et al.*, J. Phys. Chem. Lett. **5**(3), 429 (2014). Copyright 2014 American Chemical Society. The black squares in (c) and (d) show the measurements of the perovskites in PMMA; blue triangles perovskites with the electron acceptor (phenyl-C_{61}-butyric acid methyl ester, PCBM); and red circles perovskites with the hole acceptor spiro-OMeTAD (2,2′,7,7′-tetrakis(N,N′-di-p-methoxyphenylamine)-9,9′-spirobifluorene), respectively, along with the exponential fits. The insert in (c) compares the recombination lifetimes for $CH_3NH_3PbI_{3-x}Cl_x$ and $CH_3NH_3PbI_3$ in PMMA. Reprinted with permissionStranks *et al.*, Science **342**(6156), 341 (2013). Copyright 2014 American Association for the Advancement of Science.

was measured to be around 0.1 μm,[7,8] slightly larger for electrons than for holes. $CH_3NH_3PbI_{3-x}Cl_x$ has a much larger recombination lifetime than $CH_3NH_3PbI_3$,[51] the difference is more than an order of magnitude for perovskite on glass embedded in poly(methylmethacrylate) (PMMA). While the addition of electron and hole acceptor materials accelerates the photoluminescence for both perovskites, the quenched fraction of photoluminescence of $CH_3NH_3PbI_{3-x}Cl_x$ is much higher. This result agrees with the higher estimated effective masses for holes compared to electrons.[52] It has to be noted that these results were not measured using a complete device but perovskite and electron- or hole-transport layers.[7] Measurements using electron beam-induced current (EBIC) of complete devices show a much larger diffusion length for $CH_3NH_3PbI_3$.[5] Figs. 4(a) and 4(b) show a scanning electron microscopy images and EBIC for a pure and mixed halide perovskites. The EBIC measurement of $CH_3NH_3PbI_{3-x}Cl_x$ and $CH_3NH_3PbI_3$ show current generation in the entire absorber.[5] Charge separation occurs in the $CH_3NH_3PbI_{3-x}Cl_x$ layer with two maxima, indicated by the green and blue arrows: These maxima at the absorber/hole conductor interface (green) and absorber/electron conductor (blue) show the prime charge separation regions in the device with the peak at the absorber/hole-conductor slightly higher than at the absorber/electron-conductor interface. For $CH_3NH_3PbI_3$, the peak of charge separation at the absorber/electron-conductor interface (green) dominates the absorber/hole conductor interface (blue). For $CH_3NH_3PbI_{3-x}Cl_x$, measurements of the diffusion length using results from EBIC indicate an effective diffusion length of 1.9 μm for electrons and 1.2 μm for holes.[5] Comparison of the EBIC measurement for $CH_3NH_3PbI_{3-x}Cl_x$ and $CH_3NH_3PbI_3$ indicates a larger diffusion length for holes compared to electrons, much larger than reported by Stranks *et al.* or Xing *et al.*[7,8] Comparison of the diffusion length obtained from photoluminescence decay and EBIC measurement show a higher diffusion length of $CH_3NH_3PbI_{3-x}Cl_x$ compared to $CH_3NH_3PbI_3$,[5,7] but indicate that the transport properties of perovskite are not fully understood. The mechanism of chlorine incorporation (better crystal formation or actual doping) also remains unclear. However, as

noted above, an increased conductivity (inverse series resistance) was measured for the mixed halide with a low chlorine percentage in $CH_3NH_3PbI_{3-x}Cl_x$, indicating doping.[15]

Measurements of the diffusion length via photoluminescence decay for the formamidinium perovskite $HC(NH_2)_2PbI_3$ gives electron diffusion length of ~180 nm and hole diffusion length of ~810 nm.[38] Recent results of impedance spectroscopy measurements[6] indicate that the combination of a mesoporous TiO_2 nanostructure and $CH_3NH_3PbI_3$ enhances the diffusion length of charge carriers, comparable to $CH_3NH_3PbI_{3-x}Cl_x$, which explains similar performance values for the highest-developed solar cells for both designs.

The exciton binding energy of the perovskite is related to the dielectric response of the material and there is evidence that the nature of the exciton in the perovskite is more *Wannier*-like.[16,37,53] Simulated values for the static ϵ_0 and high-frequency constant ϵ_∞ are similar to values of other bulk absorber materials used for photovoltaic applications like CdTe.[37,44] Exciton binding energies were measured to be between 35 and 50 meV for the low-temperature γ-phase of $CH_3NH_3PbI_3$.[35,54] $CH_3NH_3PbI_{3-x}Cl_x$ and $CH_3NH_3PbI_3$ in a mesoporous nanostructure both show a strong photoluminescence peak between 750 and 800 nm associated with stimulated emission of the perovskite.[25,55] Fitting the integration of the photoluminescence for temperatures down to 170 K (still the tetragonal β-phase) for $CH_3NH_3PbI_{3-x}Cl_x$ indicates higher exciton binding energies of about 100 meV assuming that the photoluminescence is dominated by exciton recombination.[55] For a bulk $CH_3NH_3PbI_3$, no photoluminescence could be detected[25] indicating no significant radiative recombination. Other effects like a frequency shift of the absorption onset between bulk perovskite and perovskite in a mesoporous film, quantum confinement, or dielectric environment of the mesoporous film also need to be considered for a comparison of the different results of the binding energy as well as the increased defect- and surface-related recombination for perovskite in mesoporous nanostructures. However, the absence of photoluminescence for bulk $CH_3NH_3PbI_3$[25] indicates the direct generation of free charge carriers upon illumination. The corresponding *Bohr*-radius for the lower exciton binding energy of about 50 meV would be 26 Å, thus covering the area of more than two unit cells of the pseudo-cubic structure; the *Bohr*-radius could explain quantum confinement effects in the mesoporous film, since the pore size is similar to the *Bohr*-radius. For one- and two-dimensional perovskites with larger organic cations, the binding energy is much larger compared to the three-dimensional perovskites, since quantum confinement in the few-layer quantum well structures has stronger influence on the excitons.[35]

Since the methylammonium cations are polar by themselves and bonded via hydrogen bonds and ionic effects, they can easily reorient within the lattice of inorganic octahedra. The reorientation of the dipoles and lattice distortion due to the polar nature of the octahedra are the origin of some effects of the lead halide perovskites. For instance, the absolute resistance shows a non-ohmic hysteresis, which can be attributed to the reorientation of the methylammonium cations of the perovskite under the influence of an external field.[33] These ferroelectric effects introduce inductance and/or capacitance within the system, producing a large density of states within the perovskite, which separates this system from the class of hybrid dye-sensitized solar cells.[19,33] In addition to the polar nature of the lattice itself, the polarity of the organic cations has a number of important effects on solar cell performance. The electronic polarization of $CH_3NH_3PbI_3$ and $HC(NH_2)_2PbI_3$ is comparable to the polarization of materials, which show above-bandgap voltages.[56] Charge carriers in a ferroelectric material like perovskite can diffuse via grain boundaries to the electrodes of the device. As reported by Choi *et al.*,[25] a large fraction of the perovskite consists of small crystallites, which could form ferroelectric domains.[56] In a multi-domain perovskite crystal, electrons would move along the minima of the electric field and holes along the maxima, thus reducing recombination due to spatial separation of the charge carriers.[56] As an external field would influence domain orientation and charge density at the boundaries, a hysteretical behaviour could be expected.[19,56] At the moment, however, the influence of the ferroelectricity of lead halide perovskites on the device function is not understood and further research is necessary in order to shed light on ferroelectric phenomena in perovskite photovoltaics.

The interplay between physical and electronic structure of lead halide perovskites has huge effects on the properties of the material. Table I summarizes structure and bandgap for lead halide perovskites.

TABLE I. Properties of different lead halide perovskites.

Composition	Bandgap (eV)	Structure at room temperature	Carrier diffusion length	CBM (eV)	VBM (eV)	
$CH_3NH_3PbI_3$	1.5–1.61	Tetragonal	$L_{D,e} > 0.1\ \mu m$ $L_{D,h} > 0.1\ \mu m$	−3.93	−5.3	2,5,7,57
$CH_3NH_3PbBr_3$	2.32	Cubic	...	−3.36	−5.58	20
$CH_3NH_3PbCl_3$	3.1	Cubic	...			49
$CH_3NH_3PbI_{3-x}Cl_x$	1.55–1.64	Tetragonal	$L_{D,e}$ 1.9 μm $L_{D,h}$ 1.2 μm	−3.75	−5.43	5,9,13,15
$CH_3NH_3PbI_{3-x}Br_x$	1.5–2.32	Tetragonal/cubic, turnover $x \sim 0.2$	...	...	...	20
$HC(NH_2)_2PbI_3$	1.47	Tetragonal	$L_{D,e}$ 0.2 μm $L_{D,h}$ 0.8 μm	−4.2	−5.7	38,51
$HC(NH_2)_2PbBr_3$	2.23	Cubic	...	...	...	38

Although pure as well as mixed lead halide perovskites have been successfully implemented in high-efficiency photovoltaic devices, the incorporation- mechanism of chlorine into the pure halide perovskite $CH_3NH_3PbI_3$ and its effects are not clear yet. Understanding the effects of added chlorine to the perovskite such as increased carrier diffusion length and conductivity in combination with a nearly identical bandgap is essential for further development of metal-organic halide perovskites for solar cell applications. Taking advantage of the good control over the doping level of these materials could allow the fabrication of p-n-junction perovskite cells and open new synthesis routes aside inorganic-organic or depleted inorganic heterojunction devices. A perovskite homojunction cell is potentially easier to fabricate and might help to further lower the projected mass production costs of this fascinating technology. Furthermore, a deeper understanding of the impact of the perovskite composition on the crystal formation and the electronic structure of the material will enable the optimization of current lead halide perovskites and will very likely allow efficiencies exceeding 20% in the near future. More importantly, the knowledge gained about the lead halide perovskites can be possible transferred to lead-free perovskites, which are the next logical step towards non-toxic low-cost high-efficiency materials for thin film photovoltaics.

The authors would like to thank Maren Frei, Martin Putnik, Eugen Zimmerman, Philipp Ehrenreich, and Tom Kollek for fruitful discussions. J.W. acknowledges support by the German Research Foundation (DFG) in the project "Identification and overcoming of loss mechanisms in nanostructured hybrid solar cells—pathways towards more efficient devices." J.A.D. would like to thank the Humboldt Foundation for supporting his research.

[1] A. Kojima, K. Teshima, Y. Shirai, and T. Miyasaka, J. Am. Chem. Soc. **131**(17), 6050 (2009).
[2] H. S. Kim, C. R. Lee, J. H. Im, K. B. Lee, T. Moehl, A. Marchioro, S. J. Moon, R. Humphry-Baker, J. H. Yum, J. E. Moser, M. Grätzel, and N. G. Park, Sci. Rep. **2**, 591 (2012).
[3] M. M. Lee, J. Teuscher, T. Miyasaka, T. N. Murakami, and H. J. Snaith, Science **338**(6107), 643 (2012).
[4] Research Cell Efficiency Records, National Center for Photovoltaics, see http://www.nrel.gov/ncpv/images/efficiency_chart.jpg, 10.02.2014.
[5] E. Edri, S. Kirmayer, A. Henning, S. Mukhopadhyay, K. Gartsman, Y. Rosenwaks, G. Hodes, and D. Cahen, Nano Lett. **14**(2), 1000 (2014).
[6] V. Gonzalez-Pedro, E. J. Juarez-Perez, W. S. Arsyad, E. M. Barea, F. Fabregat-Santiago, I. Mora-Sero, and J. Bisquert, Nano Lett. **14**(2), 888 (2014).
[7] S. D. Stranks, G. E. Eperon, G. Grancini, C. Menelaou, M. J. P. Alcocer, T. Leijtens, L. M. Herz, A. Petrozza, and H. J. Snaith, Science **342**(6156), 341 (2013).
[8] G. Xing, N. Mathews, S. Sun, S. S. Lim, Y. M. Lam, M. Grätzel, S. Mhaisalkar, and T. C. Sum, Science **342**(6156), 344 (2013).
[9] B. Conings, L. Baeten, C. De Dobbelaere, J. D'Haen, J. Manca, and H.-G. Boyen, Adv. Mater. **26**, 2041 (2014).
[10] P. Docampo, J. M. Ball, M. Darwich, G. E. Eperon, and H. J. Snaith, Nat. Commun. **4**, 2761 (2013); G. E. Eperon, V. M. Burlakov, P. Docampo, A. Goriely, and H. J. Snaith, Adv. Funct. Mat. **24**(1), 151 (2014); D. Liu and T. L. Kelly, Nat. Photon. **8**(2), 133 (2014); O. Malinkiewicz, A. Yella, Y. H. Lee, G. M. Espallargas, M. Grätzel, M. K. Nazeeruddin, and H. J. Bolink, *ibid.* **8**(2), 128 (2014).
[11] M. Liu, M. B. Johnston, and H. J. Snaith, Nature (London) **501**(7467), 395 (2013).
[12] J. You, Z. Hong, Y. M. Yang, Q. Chen, M. Cai, T. B. Song, C. C. Chen, S. Lu, Y. Liu, H. Zhou, and Y. Yang, ACS Nano **8**(2), 1674 (2014).
[13] J. M. Ball, M. M. Lee, A. Hey, and H. J. Snaith, Energy Environ. Sci. **6**(6), 1739 (2013).
[14] J. Burschka, N. Pellet, S. J. Moon, R. Humphry-Baker, P. Gao, M. K. Nazeeruddin, and M. Grätzel, Nature (London) **499**(7458), 316 (2013).

[15] S. Colella, E. Mosconi, P. Fedeli, A. Listorti, F. Gazza, F. Orlandi, P. Ferro, T. Besagni, A. Rizzo, G. Calestani, G. Gigli, F. De Angelis, and R. Mosca, Chem. Mater. **25**(22), 4613 (2013).
[16] E. Edri, S. Kirmayer, D. Cahen, and G. Hodes, J. Phys. Chem. Lett. **4**(6), 897 (2013).
[17] L. Etgar, P. Gao, Z. Xue, Q. Peng, A. K. Chandiran, B. Liu, M. K. Nazeeruddin, and M. Grätzel, J. Am. Chem. Soc. **134**(42), 17396 (2012); J. T.-W. Wang, J. M. Ball, E. M. Barea, A. Abate, J. A. Alexander-Webber, J. Huang, M. Saliba, I. Mora-Sero, J. Bisquert, H. J. Snaith, and R. J. Nicholas, Nano Lett. **14**, 724 (2014); K. Wojciechowski, M. Saliba, T. Leijtens, A. Abate, and H. J. Snaith, Energy Environ. Sci. **7**(3), 1142 (2014).
[18] J. H. Heo, S. H. Im, J. H. Noh, T. N. Mandal, C. S. Lim, J. A. Chang, Y. H. Lee, H. J. Kim, A. Sarkar, M. K. Nazeeruddin, M. Grätzel, and S. I. Seok, Nat. Photon. **7**(6), 486 (2013).
[19] H. S. Kim, I. Mora-Sero, V. Gonzalez-Pedro, F. Fabregat-Santiago, E. J. Juarez-Perez, N. G. Park, and J. Bisquert, Nat. Commun. **4**, 2242 (2013).
[20] J. H. Noh, S. H. Im, J. H. Heo, T. N. Mandal, and S. I. Seok, Nano Lett. **13**(4), 1764 (2013).
[21] E. Edri, S. Kirmayer, M. Kulbak, G. Hodes, and D. Cahen, J. Phys. Chem. Lett. **5**(3), 429 (2014).
[22] H.-S. Kim, J.-W. Lee, N. Yantara, P. P. Boix, S. A. Kulkarni, S. Mhaisalkar, M. Grätzel, and N.-G. Park, Nano Lett. **13**(6), 2412 (2013); M. H. Kumar, N. Yantara, S. Dharani, M. Grätzel, S. Mhaisalkar, P. P. Boix, and N. Mathews, Chem. Commun. **49**(94), 11089 (2013); J. Qiu, Y. Qiu, K. Yan, M. Zhong, C. Mu, H. Yan, and S. Yang, Nanoscale **5**(8), 3245 (2013).
[23] W. A. Laban and L. Etgar, Energy Environ. Sci. **6**(11), 3249 (2013).
[24] Q. Chen, H. Zhou, Z. Hong, S. Luo, H.-S. Duan, H.-H. Wang, Y. Liu, G. Li, and Y. Yang, J. Am. Chem. Soc. **136**(2), 622 (2014).
[25] J. J. Choi, X. Yang, Z. M. Norman, S. J. L. Billinge, and J. S. Owen, Nano Lett. **14**(1), 127 (2014).
[26] D. Q. Bi, S. J. Moon, L. Haggman, G. Boschloo, L. Yang, E. M. J. Johansson, M. K. Nazeeruddin, M. Grätzel, and A. Hagfeldt, RSC Adv. **3**(41), 18762 (2013).
[27] H. J. Snaith, J. Phys. Chem. Lett. **4**(21), 3623 (2013).
[28] N.-G. Park, J. Phys. Chem. Lett. **4**(15), 2423 (2013).
[29] H.-S. Kim, S. H. Im, and N.-G. Park, J. Phys. Chem. C **118**, 5615 (2014).
[30] J. W. Anthony, R. A. Bideaux, K. W. Bladh, and M. C. Nichols, *Handbook of Mineralogy* (Mineralogical Society of America, 2005).
[31] I. Chung, J.-H. Song, J. Im, J. Androulakis, C. D. Malliakas, H. Li, A. J. Freeman, J. T. Kenney, and M. G. Kanatzidis, J. Am. Chem. Soc. **134**(20), 8579 (2012).
[32] D. D. Fong, G. B. Stephenson, S. K. Streiffer, J. A. Eastman, O. Auciello, P. H. Fuoss, and C. Thompson, Science **304**(5677), 1650 (2004); A. P. Mackenzie, S. R. Julian, A. J. Diver, G. J. McMullan, M. P. Ray, G. G. Lonzarich, Y. Maeno, S. Nishizaki, and T. Fujita, Phys. Rev. Lett. **76**(20), 3786 (1996); Y. Moritomo, A. Asamitsu, H. Kuwahara, and Y. Tokura, Nature (London) **380**(6570), 141 (1996); A. Bhatnagar, A. Roy Chaudhuri, Y. Heon Kim, D. Hesse, and M. Alexe, Nat. Commun. **4**, 2835 (2013); S. Y. Yang, J. Seidel, S. J. Byrnes, P. Shafer, C. H. Yang, M. D. Rossell, P. Yu, Y. H. Chu, J. F. Scott, J. W. Ager, L. W. Martin, and R. Ramesh, Nat. Nano **5**(2), 143 (2010).
[33] C. C. Stoumpos, C. D. Malliakas, and M. G. Kanatzidis, Inorg. Chem. **52**(15), 9019 (2013).
[34] I. Chung, B. Lee, J. He, R. P. H. Chang, and M. G. Kanatzidis, Nature (London) **485**(7399), 486 (2012).
[35] T. Ishihara, J. Lumin. **60–61**, 269 (1994).
[36] T. Baikie, Y. Fang, J. M. Kadro, M. Schreyer, F. Wei, S. G. Mhaisalkar, M. Grätzel, and T. J. White, J. Mater. Chem. A **1**(18), 5628 (2013).
[37] F. Brivio, A. B. Walker, and A. Walsh, APL Mater. **1**(4), 042111 (2013).
[38] G. E. Eperon, S. D. Stranks, C. Menelaou, M. B. Johnston, L. M. Herz, and H. J. Snaith, Energy Environ. Sci. **7**, 982 (2014).
[39] Y. Chang, C. Park, and K. Matsuishi, J. Korean Phys. Soc. **44**(4), 889 (2004).
[40] E. Mosconi, A. Amat, M. K. Nazeeruddin, M. Grätzel, and F. De Angelis, J. Phys. Chem. C **117**(27), 13902 (2013).
[41] E. Riedel and H.-J. Meyer, *Allgemeine und Anorganische Chemie*, 11th ed. (De Gruyter, 2013), p.75.
[42] L. Lang, J.-H. Yang, H.-R. Liu, H. J. Xiang, and X. G. Gong, Phys. Lett. A **378**(3), 290 (2014).
[43] D. B. Mitzi, K. Chondroudis, and C. R. Kagan, IBM J. Res. Dev. **45**(1), 29 (2001).
[44] F. Brivio, K. T. Butler, A. Walsh, and M. van Schilfgaarde, preprint arXiv:1401.6993v3 (2014).
[45] J. Even, L. Pedesseau, J.-M. Jancu, and C. Katan, J. Phys. Chem. Lett. **4**(17), 2999 (2013).
[46] R. Lindblad, D. Bi, B.-W. Park, J. Oscarsson, M. Gorgoi, H. Siegbahn, M. Odelius, E. M. J. Johansson, and H. Rensmo, J. Phys. Chem. Lett. **5**, 648 (2014).
[47] L. Etgar, Materials **6**(2), 445 (2013).
[48] A. Abrusci, S. D. Stranks, P. Docampo, H.-L. Yip, A. K. Y. Jen, and H. J. Snaith, Nano Lett. **13**(7), 3124 (2013).
[49] N. Kitazawa, Y. Watanabe, and Y. Nakamura, J. Mater. Sci. **37**(17), 3585 (2002).
[50] T. M. Koh, K. Fu, Y. Fang, S. Chen, T. C. Sum, N. Mathews, S. G. Mhaisalkar, P. P. Boix, and T. Baikie, "Formamidinium-Containing Metal-Halide: An Alternative Material for Near-IR Absorption Perovskite Solar Cells," J. Phys. Chem. C (published online).
[51] C. Wehrenfennig, G. E. Eperon, M. B. Johnston, H. J. Snaith, and L. M. Herz, Adv. Mater. **26**, 1584 (2014).
[52] G. Giorgi, J.-I. Fujisawa, H. Segawa, and K. Yamashita, J. Phys. Chem. Lett. **4**(24), 4213 (2013).
[53] K. Tanaka, T. Takahashi, T. Ban, T. Kondo, K. Uchida, and N. Miura, Solid State Commun. **127**(9), 619 (2003).
[54] M. Hirasawa, T. Ishihara, T. Goto, K. Uchida, and N. Miura, Physica B **201**, 427 (1994).
[55] W. Zhang, M. Saliba, S. D. Stranks, Y. Sun, X. Shi, U. Wiesner, and H. J. Snaith, Nano Lett. **13**(9), 4505 (2013).
[56] J. M. Frost, K. T. Butler, F. Brivio, C. H. Hendon, M. van Schilfgaarde and A. Walsh, preprint arXiv:1402.4980v2 (2014).
[57] Y. Yasuhiro, N. Toru, E. Masaru, W. Atsushi, and K. Yoshihiko, Appl. Phys. Exp. **7**(3), 032302 (2014).